VOLUME 113, NUMBER 12
JUNE 5, 1991

JOURNAL
OF THE
AMERICAN
CHEMICAL
SOCIETY

Intramolecular Motions of a Zinc Finger DNA-Binding Domain from Xfin Characterized by Proton-Detected Natural Abundance ^{13}C Heteronuclear NMR Spectroscopy

Arthur G. Palmer III, Mark Rance, and Peter E. Wright*

Contribution from the Department of Molecular Biology, Research Institute of Scripps Clinic, 10666 North Torrey Pines Road, La Jolla, California 92037. *Received November 13, 1990*

Abstract: The zinc finger DNA-binding domain Xfin-31 is a 25-residue peptide that binds a single zinc atom and forms a compact globular structure in solution. To characterize the intramolecular dynamics of Xfin-31, the ^{13}C spin–lattice and spin–spin relaxation rate constants and the $\{^1H\}$–^{13}C nuclear Overhauser effect (NOE) enhancements have been measured for the backbone and side chain methine carbons by two-dimensional proton-detected heteronuclear NMR spectroscopy at a ^{13}C Larmor frequency of 125 MHz and natural ^{13}C abundance. The relaxation rate constants and the NOE enhancements have been analyzed by using a model-free formalism that depends on the overall rotational correlation time of the molecule, τ_m, the order parameter S, and effective internal correlation time, τ_e, for each methine carbon. The optimized global value of τ_m is 1.88 ± 0.02 ns. The backbone C^α carbons are grouped into four categories based on the values of the order parameters: the N-terminal residue Tyr^1 with $S^2 = 0.73 \pm 0.04$; the C-terminal residues Lys^{24} and Asn^{25} with $S^2 < 0.5$; residues Phe^{10}-Lys^{13} with an average $S^2 = 0.77 \pm 0.03$; and the remainder of the backbone carbon nuclei with an average $S^2 = 0.89 \pm 0.05$. For the side chain C^β of Val^{11} and Val^{22} and the C^γ of Leu^5, the values of S^2 are 0.62 ± 0.03, 0.66 ± 0.04, and 0.47 ± 0.03, respectively. Estimates of τ_e could be obtained for 13 of the backbone and 3 of the side chain methine carbons. Excluding the terminal residues, the average value of τ_e for the backbone carbon nuclei was 34 ± 16 ps. With the exception of the terminal residues, the motions of the backbone carbon nuclei of Xfin-31 are highly restricted. Residues 10–13, which form a turn between the β-sheet and the helix present in the three-dimensional structure of Xfin-31, have a slightly higher mobility than the rest of the interior backbone, and the two residues at the C-terminus have considerable conformational flexibility. The side chains of the hydrophobic Val and Leu residues are more mobile than the backbone but are still significantly restricted, which indicates that Xfin-31 is compact despite its small size. Systematically large spin–spin relaxation rates for residues in the zinc binding site imply that conformational exchange may occur in this region on a time scale longer than the overall rotational correlation time.

Introduction

The nature and rates of the intramolecular motions of proteins have been the subjects of intense theoretical and experimental interest both because of their central importance to biological functions,[1-5] including enzyme catalysis, allosterism, and ligand binding, and because of their influence on the fundamental physicochemical properties of proteins.[6-9] Such motions reflect both random equilibrium fluctuations and responses to perturbations, such as changes in ionization or temperature and interactions with specific ligands. Internal motions in proteins occur

(1) Gurd, F. R. N.; Rothgeb, T. M. *Adv. Prot. Chem.* **1979**, *33*, 73–165.
(2) Welch, G. R.; Somogyi, B.; Damjanovich, S. *Prog. Biophys. Molec. Biol.* **1982**, *39*, 109–146.
(3) Bennett, W. S.; Huber, R. *CRC Crit. Rev. Biochem.* **1983**, *15*, 290–384.
(4) Ringe, D.; Petsko, G. *Prog. Biophys. Molec. Biol.* **1985**, *45*, 197–235.
(5) Williams, R. J. P. *Eur. J. Biochem.* **1989**, *183*, 479–497.
(6) Careri, G.; Gratton, E. In *The Fluctuating Enzyme*; Welch, G. R., Ed.; Wiley: New York, 1986; pp 227–262.
(7) Brooks, C. L.; Karplus, M.; Pettitt, B. M. *Adv. Chem. Phys.* **1988**, *71*, 1–259.
(8) Frauenfelder, H.; Parak, F.; Young, R. D. *Annu. Rev. Biophys. Biophys. Chem.* **1988**, *17*, 451–479.
(9) Wodak, S. J.; DeCrombrogghe, M.; Janin, J. *Prog. Biophys. Molec. Biol.* **1987**, *49*, 29–63.

0002-7863/91/1513-4371$02.50/0

with widely different temporal and spatial characteristics and include bond vibrations and rotations; librational motions of the protein backbone; local oscillations of small groups of atoms, such as amino acid side chains; and concerted segmental motions of groups of residues, such as relative movements of secondary structures or domains. Internal motions with characteristic times in the subpicosecond and picosecond regimes generally represent low-amplitude fluctuations around locally favorable conformations or between conformational substates separated by potential energy barriers that are smaller than or comparable to thermal energies. In the nanosecond and longer temporal regimes, activated processes, in which a larger potential energy barrier exists between conformational states, become dominant.

As befits the significance of internal motions in proteins, a number of experimental and theoretical methods have been developed that are capable of characterizing these motions. Experimental techniques include fluorescence,[10,11] Mössbauer,[12,13] and nuclear magnetic resonance (NMR)[5,14,15] spectroscopies; neutron[16-18] and X-ray[19,20] scattering; and isotope exchange measurements.[21,22] Theoretical methods include normal mode analysis[23-25] and molecular dynamics simulations.[7,26,27] Of the different experimental techniques, NMR spectroscopy is uniquely capable of comprehensively characterizing the internal motions of proteins in solution at the atomic level over time scales ranging from picoseconds to hours. In approximate order of the accessible temporal regimes, applicable NMR techniques include relaxation rate measurements,[28-30] dynamic NMR and line shape analysis,[31] magnetization transfer experiments,[32,33] and amide isotope exchange measurements.[14,22,34]

For diamagnetic proteins in isotropic solution, the primary mechanism of nuclear magnetic relaxation of protonated ^{13}C nuclei, at natural abundance, and of ^{15}N nuclei is the dipolar interaction with the directly attached protons; at high magnetic field strengths, chemical shift anisotropy (CSA) also contributes to the relaxation of these heteronuclei.[35] The relaxation rates are governed by the internal motions and overall rotational motions of the molecules; consequently, characterization of ^{13}C and ^{15}N heteronuclear relaxation can provide information about internal dynamics of proteins on time scales faster than the rotational correlation time.[28,36] Heteronuclear relaxation can be interpreted with use of specific models for internal motions, such as restricted diffusion and site jump models;[28,37] however, model-free formal methods[36,38-41] are preferable, at least for the initial analysis, because the available experimental data are generally insufficient to completely characterize complex internal motions or to uniquely determine a specific motional model. Molecular dynamics simulations provide a complementary approach for the interpretation of relaxation measurements but have not yet been widely applied.[42-44]

Although the potential of investigations of heteronuclear magnetic relaxation in proteins has been recognized and numerous studies have been performed over the past two decades,[45-54] until recently, applications were severely hindered by the low natural abundance and inherent lack of sensitivity of ^{13}C and ^{15}N nuclei and by the limited resolution achievable with one-dimensional NMR spectroscopy. These problems have been mitigated by proton-detected heteronuclear NMR techniques,[55-58] which enable heteronuclei to be indirectly monitored with increased sensitivity; by two-dimensional NMR spectroscopy,[59] which affords the increased resolution of a second frequency dimension; and by the methods of genetic engineering,[60] which greatly facilitate the

(10) Lakowicz, J. *Methods Enzymol.* **1986**, *131*, 518-567.
(11) Bucci, E.; Steiner, R. F. *Biophys. Chem.* **1988**, *30*, 199-224.
(12) Parak, F.; Reinisch, L. *Methods Enzymol.* **1986**, *131*, 568-607.
(13) Goldanskii, V. I.; Krupyanskii, Y. F. *Q. Rev. Biophys.* **1989**, *22*, 39-92.
(14) Wagner, G. *Q. Rev. Biophys.* **1983**, *16*, 1-57.
(15) Jardetzky, O.; Roberts, G. C. K. *NMR in Molecular Biology*; Academic Press: New York, 1981.
(16) Cusack, S. *Comm. Mol. Cell. Biophys.* **1986**, *3*, 243-271.
(17) Middendorf, H. D. *Annu. Rev. Biophys. Bioeng.* **1984**, *13*, 425-451.
(18) Kossiakoff, A. A. *Methods Enzymol.* **1986**, *131*, 433-447.
(19) Ringe, D.; Petsko, G. A. *Methods Enzymol.* **1986**, *131*, 389-433.
(20) Ichiye, T.; Karplus, M. *Biochemistry* **1988**, *27*, 3487-3497.
(21) Gregory, R. B.; Rosenberg, A. *Methods Enzymol.* **1986**, *131*, 448-508.
(22) Englander, S. W.; Kallenbach, N. R. *Q. Rev. Biophys.* **1984**, *16*, 521-655.
(23) Brooks, B. R.; Karplus, M. *Proc. Natl. Acad. Sci. U.S.A.* **1983**, *80*, 6571-6575.
(24) Go, N.; Noguti, T.; Nishikawa, T. *Proc. Natl. Acad. Sci. U.S.A.* **1983**, *80*, 3696-3700.
(25) Levitt, M. *J. Biol. Chem.* **1983**, *168*, 621-657.
(26) Karplus, M.; McCammon, J. A. *Annu. Rev. Biochem.* **1983**, *52*, 263-300.
(27) McCammon, J. A.; Harvey, S. C. *Dynamics of Proteins and Nucleic Acids*; Cambridge University Press: Cambridge, 1987.
(28) London, R. E. In *Magnetic Resonance in Biology*; Cohen, J. S., Ed.; Wiley: New York, 1980; pp 1-69.
(29) Keniry, M. A. *Methods Enzymol.* **1989**, *176*, 376-386.
(30) Opella, S. J. *Methods Enzymol.* **1986**, *131*, 327-361.
(31) Rao, B. D. N. *Methods Enzymol.* **1989**, *176*, 279-311.
(32) Led, J. J.; Gesmar, H.; Abildgaard, F. *Methods Enzymol.* **1989**, *176*, 311-329.
(33) Alger, J. R.; Shulman, R. G. *Q. Rev. Biophys.* **1984**, *17*, 83-124.
(34) Roder, H. *Methods Enzymol.* **1989**, *176*, 446-473.
(35) Abragam, A. *Principles of Nuclear Magnetism*; Claredon Press: Oxford, 1961; pp 264-353.
(36) Lipari, G.; Szabo, A. *J. Am. Chem. Soc.* **1982**, *104*, 4546-4559.
(37) Heatley, F. In *Annual Reports on NMR Spectroscopy*; Webb, G. A., Ed.; Academic Press: London, 1986; Vol. 17, pp 179-230.
(38) Lipari, G.; Szabo, A. *J. Am. Chem. Soc.* **1982**, *104*, 4559-4570.
(39) Fedotov, V. D.; Kivayeva, L. S. *J. Biol. Struct. Dynamics* **1987**, *4*, 599-619.
(40) Zang, L.; Laughlin, M. R.; Rothman, D. L.; Shulman, R. G. *Biochemistry* **1990**, *29*, 6815-6820.
(41) Clore, G. M.; Szabo, A.; Bax, A.; Kay, L. E.; Driscoll, P. C.; Gronenborn, A. M. *J. Am. Chem. Soc.* **1990**, *112*, 4989-4991.
(42) Levy, R. M.; Karplus, M.; Wolynes, P. G. *J. Am. Chem. Soc.* **1981**, *103*, 5998-6011.
(43) Olejniczak, E. T.; Dobson, C. M.; Karplus, M.; Levy, R. M. *J. Am. Chem. Soc.* **1984**, *106*, 1923-1930.
(44) Kessler, H.; Griesinger, C.; Lautz, J.; Müller, A.; van Gunsteren, W. F.; Berendsen, H. J. C. *J. Am. Chem. Soc.* **1988**, *110*, 3393-3396.
(45) Allerhand, A.; Doddrell, D.; Glushko, V.; Cochran, D. W.; Wenkert, E.; Lawson, P. J.; Gurd, F. R. N. *J. Am. Chem. Soc.* **1971**, *93*, 544-546.
(46) Glushko, V.; Lawson, P. J.; Gurd, F. R. N. *J. Biol. Chem.* **1972**, *247*, 3176-3185.
(47) Gust, D.; Moon, R. B.; Roberts, J. D. *Proc. Natl. Acad. Sci. U.S.A.* **1975**, *72*, 4696-4700.
(48) Norton, R. S.; Clouse, A. O.; Addleman, R.; Allerhand, A. *J. Am. Chem. Soc.* **1977**, *99*, 79-83.
(49) Richarz, R.; Nagayama, K.; Wüthrich, K. *Biochemistry* **1980**, *19*, 5189-5196.
(50) Hughes, L. T.; Cohen, J. S.; Szabo, A.; Niu, C.; Matsuura, S. *Biochemistry* **1984**, *23*, 4390-4394.
(51) Henry, G. D.; Weiner, J. H.; Sykes, B. D. *Biochemistry* **1986**, *25*, 590-598.
(52) Hawkes, G. E.; Lian, L.; Randall, E. W.; Sales, K. D.; Curzon, E. H. *Eur. J. Biochem.* **1987**, *166*, 437-445.
(53) McCain, D. C.; Ulrich, E. L.; Markley, J. L. *J. Magn. Reson.* **1988**, *80*, 296-305.
(54) Dellwo, M. J.; Wand, A. J. *J. Am. Chem. Soc.* **1989**, *111*, 4571-4578.
(55) Sklenar, V.; Torchia, D.; Bax, A. *J. Magn. Reson.* **1987**, *73*, 375-379.
(56) Kay, L. E.; Jue, T. L.; Bangerter, B.; Demou, P. C. *J. Magn. Reson.* **1987**, *73*, 558-564.
(57) Nirmala, N. R.; Wagner, G. *J. Am. Chem. Soc.* **1988**, *110*, 7557-7558.
(58) Nirmala, N. R.; Wagner, G. *J. Magn. Reson.* **1989**, *82*, 659-661.
(59) Ernst, R. R.; Bodenhausen, G.; Wokaun, A. *Principles of Nuclear Magnetic Resonance in One and Two Dimensions*; Claredon Press: Oxford, 1987.

isotopic enrichment of proteins. Recently, investigations of heteronuclear relaxation have been reported for the α ^{13}C in bovine pancreatic trypsin inhibitor at natural ^{13}C abundance[57] and for the amide ^{15}N in uniformly enriched staphylococcal nuclease[61] and interleukin-1β.[62]

The zinc finger is a structural motif that is capable of binding nucleic acids and is recurrent in regulatory proteins that recognize specific sequences of DNA and RNA.[63,64] Xfin-31 is a 25-residue synthetic zinc finger peptide derived from the consensus sequence of the *Xenopus laevis* protein Xfin. The three-dimensional structure of the zinc complex of Xfin-31 has been determined by ^1H NMR spectroscopy.[65] The peptide has a compact globular structure in which a single zinc atom is coordinated by two cysteinyl and two histidinyl ligands. Although small, Xfin-31 displays many features typical of larger folded proteins: an antiparallel β-hairpin (residues 1–10), a helix (residues 12–24), and a closely packed hydrophobic core. Thus, Xfin-31 is well-suited for investigations of heteronuclear relaxation and internal dynamics in polypeptides.

In the present work, two-dimensional proton-detected ^{13}C NMR spectroscopy has been used to measure the spin–lattice and spin–spin relaxation rate constants and the $\{^1H\}$–^{13}C nuclear Overhauser effect (NOE) enhancements for the backbone and side chain methine carbons, except for Leu[16] C^γ, at natural ^{13}C isotopic abundance and a Larmor frequency of 125 MHz. The relaxation parameters have been analyzed with use of a model free formalism[36] to obtain the overall rotational correlation time, and the order parameters and effective internal correlation times for each methine carbon. The results show that the motions of the majority of the backbone C^α of Xfin-31 are highly restricted with $S^2 > 0.8$. Residues 10–13, which form a loop between the β-sheet and the helix in the tertiary structure of Xfin-31, the N-terminal residue, and the two residues at the C-terminus have larger amplitudes of motion than the remainder of the backbone. Larger than expected spin–spin relaxation rates are observed for residues in the zinc binding site, which may result from conformational exchange.[62] The motional characteristics of the backbone α carbons of Xfin-31 accord with the results of the studies of the dynamics of the backbone amide nitrogens in the staphylococcal nuclease[61] and interleukin-1β.[62]

Theory

Pulse sequences used for the relaxation measurements of the methine carbons of Xfin-31 are similar to those previously used for proton-detected heteronuclear relaxation experiments[55–58,61,62] and are shown in Figure 1. The experiments used to measure the spin–lattice (Figure 1a) and spin–spin (Figure 1b) relaxation rate constants consist of an initial DEPT[66] sequence to transfer magnetization from the methine proton to the carbon, a relaxation period T that is parametrically varied between two-dimensional data sets, the t_1 evolution period, and a second DEPT sequence to subsequently transfer magnetization from the methine carbon back to the proton for detection. The experiment used to measure the NOE enhancements (Figure 1c) consists of an initial relaxation delay, the t_1 evolution period, and a DEPT sequence to transfer magnetization to the methine proton for detection; spectra are acquired with and without saturation of the proton magnetization during the relaxation delay. The pulse sequences of Figure 1 are formally identical with the conventional one-dimensional inversion recovery,[67] Carr–Purcell–Meiboom–Gill (CPMG),[68] and

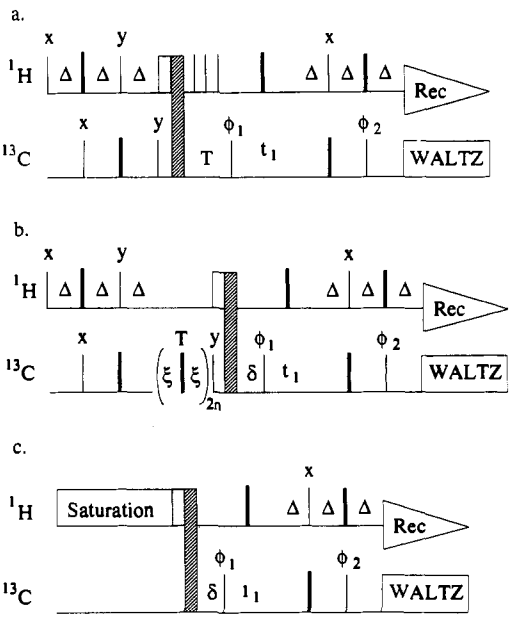

Figure 1. Pulse sequences for NMR spectroscopy. Shown are the pulse sequences for (a) ^{13}C inversion recovery, (b) ^{13}C CPMG, and (c) $\{^1H\}$–^{13}C steady-state NOE experiments designed to measure the spin–lattice and spin–spin relaxation rate constants and the NOE enhancements with two-dimensional proton-detected natural abundance ^{13}C heteronuclear correlation NMR spectroscopy. Thin and thick vertical bars represent 90° and 180° pulses, respectively; hatched bars represent 2 ms homogeneity spoiling pulses; and stippled bars represent 2 ms purge pulses applied with a field strength of 9 kHz. For polarization transfer, Δ = 3.3 ms, which is slightly less than $1/(2^1J_{CH})$. The delay δ is 8 ms to allow homogeneity recovery following gradient pulses. In sequences (a) and (b) T is parametrically varied between two-dimensional experiments. In (a) ^1H 90° pulses are applied at 5-ms intervals during T to saturate the proton spins. In (b) the delay T consists of $2n$ spin–echo sequences with ξ = 2.5 ms. For measurement of the NOE enhancements, spectra are recorded without and with (c) ^1H saturation during the recovery delay. Saturation is performed with the GARP-1 sequence[92] to minimize sample heating. WALTZ-16[93] is used to decouple carbon spins during acquisition. The phase cycling used is $\phi_1 = (x, -x, x, -x)$, $\phi_2 = (x, x, -x, -x)$ and receiver $(x, -x, -x, x)$. Quadrature detection in the ω_1 dimension was achieved by TPPI.[75] Weak presaturation of the solvent resonance was used in sequences (a) and (b).

steady-state $\{^1H\}$–^{13}C NOE techniques.[69] Consequently, the intensities of the heteronuclear resonances, $I(T)$, as a function of the parametric relaxation delay T, are described by the usual inversion recovery equation

$$I(T) = I_\infty - [I_\infty - I_0] \exp(-R_1 T) \quad (1)$$

in the two-dimensional spectra acquired with the sequence of Figure 1a, and by a single exponential decay

$$I(T) = I_0 \exp(-R_2 T) \quad (2)$$

in spectra acquired with the sequence of Figure 1b. In eqs 1 and 2, I_0 is the intensity corresponding to the ^{13}C magnetization at the beginning of the relaxation period T, I_∞ is the intensity corresponding to the steady-state value of the magnetization under the given experimental conditions, and R_1 and R_2 are the phenomenological spin–lattice and spin–spin relaxation rate constants, respectively. Similarly, the NOE enhancements η are

$$\eta = I_{sat}/I_{unsat} - 1 \quad (3)$$

in which I_{sat} and I_{unsat} are the intensities of the resonances in the spectrum obtained with and without saturation of proton magnetization, respectively. For ideal polarization transfers, $I_0 \propto (\gamma_H/\gamma_C)S_{eq}$, $I_\infty = I_{sat} \propto (1 + \eta)S_{eq}$, and $I_{unsat} \propto S_{eq}$, in which S_{eq} is the thermal equilibrium value of the ^{13}C magnetization and

(60) McIntosh, L. P.; Dahlquist, F. W. *Q. Rev. Biophys.* **1990**, *23*, 1–38.
(61) Kay, L. E.; Torchia, D. A.; Bax, A. *Biochemistry* **1989**, *28*, 8972–8979.
(62) Clore, G. M.; Driscoll, P. C.; Wingfield, P. T.; Gronenborn, A. M. *Biochemistry* **1990**, *29*, 7387–7401.
(63) Klug, A.; Rhodes, D. *Trends Biochem. Sci.* **1987**, *12*, 464–469.
(64) Berg, J. M. *Annu. Rev. Biophys. Biophys. Chem.* **1990**, *19*, 405–421.
(65) Lee, M. S.; Gippert, G. P.; Soman, K. V.; Case, D. A.; Wright, P. E. *Science* **1989**, *245*, 635–637.
(66) Doddrell, D. M.; Pegg, D. T.; Bendall, M. R. *J. Magn. Reson.* **1982**, *48*, 323–327.
(67) Vold, R. L.; Waugh, J. S.; Klein, M. P.; Phelps, D. E. *J. Chem. Phys.* **1968**, *48*, 3831–3832.
(68) Meiboom, S.; Gill, D. *Rev. Sci. Instrum.* **1958**, *29*, 688–691.
(69) Noggle, J. H.; Schirmer, R. E. *The Nuclear Overhauser Effect: Chemical Applications*; Academic Press: New York, 1971.

γ_H and γ_C are the gyromagnetic ratios of the proton and carbon, respectively.

The relaxation of protonated ^{13}C nuclei at natural abundance is mediated primarily by the dipolar interaction with the attached protons and secondarily by chemical shift anisotropy.[35] Ignoring cross-correlation effects, the apparent longitudinal relaxation rate constant is

$$R_1 = R_1^{DD} + R_1^{CSA} \quad (4)$$

in which R_1^{DD} and R_1^{CSA} are the dipolar and CSA spin–lattice relaxation rate constants, respectively. Ignoring cross-correlation effects, the apparent transverse relaxation rate constant is

$$R_2 = R_2^{DD} + R_2^{CSA} + R_a \quad (5)$$

in which R_2^{DD} and R_2^{CSA} are the dipolar and CSA transverse relaxation rate constants, respectively, and R_a is the sum of the rate constants for any other pseudo-first-order processes that contribute to R_2. For example, the magnitudes of the spin–echos in a CPMG experiment are attenuated by diffusion and chemical exchange during the spin–echo period; in this case, $R_a = R_{ex} + R_D$, in which R_{ex} and R_D are the decay rate contributions from chemical exchange and diffusion. For chemical exchange between two equally populated sites, R_{ex} depends on the intrinsic rate constant for the exchange process, k_{ex}; the chemical shift difference between the sites, ω_{ex}; and the spin echo period, ξ.[70] For $k_{ex} > \omega_{ex}$

$$R_{ex} = k_{ex} - 1/(2\xi)\ \sinh^{-1}\ [\xi k_{ex} \sinh\ (2u)/u] \quad (6)$$

in which $u = \xi(k_{ex}^2 - \omega_{ex}^2)^{1/2}$. The chemical exchange contribution to R_2 is essentially independent of ξ if $\xi k_{ex} \gg 1$ and becomes negligible only if $\xi k_{ex} \ll 1$. Assuming an axially symmetric magnetic field gradient, the diffusional contribution to R_2 is given by

$$R_D = \gamma_C^2 G^2 D \xi^2/3 \quad (7)$$

in which G is the magnetic field gradient and D is the translational diffusion coefficient of the molecule.[71,72] As shown by eqs 5–7, diffusion and chemical exchange always increase the apparent spin–spin relaxation rate constant. By choice of a suitably small ξ, the contribution from diffusion usually can be made negligible for macromolecules, but minimization of the magnetization decay due to fast chemical exchange may require impracticably short delays. More complex chemical exchange processes can generate multiexponential decay curves in spin–echo pulse sequences;[73] however detecting deviations from the monoexponential decay assumed in eq 2 is expected to be difficult for natural abundance ^{13}C spectroscopy of proteins.

For protonated ^{13}C heteronuclei at natural abundance, the dipolar relaxation rate constants are given by[35,36]

$$R_1^{DD} = (D_{CH}^2/4)[J(\omega_H - \omega_C) + 3J(\omega_C) + 6J(\omega_H + \omega_C)] \quad (8)$$

$$R_2^{DD} = (D_{CH}^2/8)[4J(0) + J(\omega_H - \omega_C) + 3J(\omega_C) + 6J(\omega_H) + 6J(\omega_H + \omega_C)] \quad (9)$$

in which

$$D_{CH} = (h/2\pi)\gamma_H\gamma_C r_{CH}^{-3}(\mu_0/4\pi) \quad (10)$$

h is Plank's constant, r_{CH} is the carbon–hydrogen bond length, μ_0 is the permeability of free space, and ω_H and ω_C are the Larmor frequencies of ^1H and ^{13}C. The spectral density function, $J(\omega)$, is the Fourier transform of the orientational correlation function for a unit vector pointing along the carbon–hydrogen bond and incorporates the dependence of the relaxation rates on molecular motion. Assuming an axially symmetric chemical shift tensor, the CSA relaxation rate constants are[35,36]

$$R_1^{CSA} = \Delta\delta^2\omega_C^2 J(\omega_C) \quad (11)$$

$$R_2^{CSA} = (\Delta\delta^2\omega_C^2/6)[4J(0) + 3J(\omega_C)] \quad (12)$$

in which $\Delta\delta = \delta_\parallel - \delta_\perp$, and $\delta_\parallel$ and $\delta_\perp$ are the parallel and perpendicular components of the chemical shift tensor. The NOE enhancement is given by[62,74]

$$\eta = \frac{\gamma_H[6J(\omega_H + \omega_C) - J(\omega_H - \omega_C)]}{\gamma_C[J(\omega_H - \omega_C) + \{3 + 4\Delta\delta^2\omega_C^2/D_{CH}^2\}J(\omega_C) + 6J(\omega_H + \omega_C)]} \quad (13)$$

If $D_{CH}^2 \gg \Delta\delta^2\omega_C^2$, then R_1^{CSA} and R_2^{CSA} can be neglected in eqs 4 and 5, and the second term in the curly brackets in eq 13 is negligible.

As shown by eqs 8–13, the relaxation parameters for the dipolar and CSA relaxation mechanisms depend on the values of the spectral density function at five characteristic frequencies. Since the available experimental data are generally insufficient to determine explicitly the spectral densities at these frequencies, the unknown spectral density function must be modelled by a simpler function that depends on a small number of physically meaningful parameters. In the model free formalism employed herein,[36] the spectral density function for the molecular motions is approximated by

$$J(\omega) = {}^2/_5\left[\frac{S^2\tau_m}{1 + (\omega\tau_m)^2} + \frac{(1 - S^2)\tau}{1 + (\omega\tau)^2}\right] \quad (14)$$

which is derived from a single exponential Padé approximation to the internal orientational correlation function. In eq 14, $\tau^{-1} = \tau_m^{-1} + \tau_e^{-1}$, τ_m is the overall rotational correlation time of the molecule, S is the order parameter, which measures the degree of spatial restriction of the unit bond vector, and τ_e is the effective internal correlation time, which is related to the characteristic temporal scale of the internal motion of the unit vector. The value of S^2 ranges from zero for internal motion that is isotropic to unity for internal motion that is completely restrained, relative to a fixed molecular frame of reference. As has been previously noted,[36] the order parameter is a model-independent measure of the restriction of the internal motion. However, the effective correlation time depends on both the amplitude and rate of the internal motion and cannot be interpreted as the characteristic time of a microscopic process without recourse to a specific motional model. In eq 14, the molecule is assumed to undergo isotropic rotational diffusion; more complex expressions have been developed for molecules whose rotational motions are highly anisotropic.[36] Extensions to this theory also have been derived that use multiexponential approximations to the internal correlation functions[41] and distribution functions for the characteristic times of internal motions.[39,40]

For purely dipolar relaxation and internal motions in the extreme narrowing limit with $\omega\tau_e \ll 1$, the ratio of the transverse to longitudinal relaxation rates for the model free spectral density function is calculated from eqs 8–10 and 14 as

$$R_2^{DD}/R_1^{DD} = (R_2^0/R_1^0)\left[\frac{1 + D_{CH}^2(1 - S^2)\tau_e/(S^2R_2^0)}{1 + D_{CH}^2(1 - S^2)\tau_e/(S^2R_1^0)}\right] \quad (15)$$

In eq 15, R_1^0 and R_2^0 are the longitudinal and transverse relaxation rates for a rigid molecule with rotational correlation time τ_m and are calculated from eqs 8–10 and 14 with $S^2 = 1$. By inspection, since $R_2^0 \geq R_1^0$, $R_2^{DD}/R_1^{DD} \leq R_2^0/R_1^0$. Consequently the apparent R_2/R_1 ratio is reduced for nuclei in which internal motions

(70) Bloom, M.; Reeves, L. W.; Wells, E. J. *J. Chem. Phys.* **1965**, *42*, 1615–1624.
(71) Hahn, E. L. *Phys. Rev.* **1950**, *80*, 580–594.
(72) Torrey, H. C. *Phys. Rev.* **1956**, *104*, 563–565.
(73) Reeves, L. W. In *Dynamic Nuclear Magnetic Resonance Spectroscopy*; Jackman, L. M., Cotton, F. A., Eds.; Academic Press: New York, 1975; pp 83–130.
(74) Weaver, A. J.; Kemple, M. D.; Prendergast, F. G. *Biophys. J.* **1988**, *54*, 1–15.

contribute strongly to the relaxation rate and increased for spins in which other decay processes contribute significantly to R_2 (eq 5). The bracketed term in eq 15 is nearly unity unless S^2 is very small; consequently, the assumption that $R_2/R_1 = R_2^{DD}/R_1^{DD} \approx R_2^0/R_1^0$ allows τ_m to be estimated.[53,61,62]

Experimental Methods

The Xfin-31 peptide (Ac-YKCGLCERSFVEKSALSRHQRVHKN-NH_2) was synthesized as described previously.[65] The sample used for NMR spectroscopy was >95% pure by analytical HPLC. The zinc complex of Xfin-31 was prepared by adding a 1.4-fold molar excess of $ZnCl_2$ to a 10 mM solution of the peptide in D_2O and adjusting the pH to 6.1 with micromolar aliquots of NaOD. The pH was measured with a glass electrode and was not corrected for isotope effects. The solution was transferred to a NMR tube, lyophilized, dissolved in D_2O, and purged with argon to remove oxygen. The NMR tube was then flame sealed.

Methine ^{13}C relaxation experiments were performed on a single sample of Xfin-31 at natural ^{13}C abundance with use of the pulse sequences of Figure 1. Spectroscopy was performed at 303 K on a Bruker AM500 spectrometer equipped with 451-MHz IF electronics. All spectra were acquired in the phase-sensitive mode by using time proportional phase incrementation (TPPI)[75] for quadrature detection in the ω_1 dimension; 2K data points were recorded in each quadrature channel during t_2 and 200 real points were recorded during t_1. Spectra were acquired with a spectral width of 5000 Hz in ω_2 and 5556 Hz in ω_1. The ^1H carrier was placed on the residual HDO resonance, and the ^{13}C carrier was set at 45.4 ppm. The ^{13}C frequency scale was indirectly referenced to TMS with use of the ^1H frequency of the residual HDO resonance.[76,77] For the R_1 and R_2 measurements, 64 scans were acquired per t_1 increment; for the NOE measurement, 128 scans were acquired per increment. For measurements of R_1 and R_2, a relaxation delay of 5.0 s, which is twice the longest ^1H longitudinal relaxation time of the methine ^{12}C isotopomers, was used between scans to ensure sufficient recovery of ^1H magnetization. In practice the recovery of proton magnetization in ^{13}C isotopomers will be significantly faster;[78] for a rigid molecule with τ_m = 1.88 ns, the longitudinal relaxation times are estimated to be reduced by factors of 2–3 due to heteronuclear dipolar relaxation. For measurements of the NOE, a relaxation delay of 4.6 s, which is greater than $10/R_1$ for the methine carbon nuclei, was used between scans to ensure that maximal NOE enhancements have developed before acquisition. For R_1 relaxation measurements, 9 separate spectra were recorded for T = 0.01, 0.05, 0.09, 0.17, 0.25, 0.45, 0.61, 1.0, and 2.0 s. For R_2 measurements, 10 spectra were recorded with T = 0.01, 0.02, 0.04, 0.07, 0.10, 0.15, 0.20, 0.30, 0.50, and 1.0 s. Four independent determinations of the NOE were made, which required eight acquisitions. Spectra were processed with the program FTNMR (Hare Research). Spectra were Fourier transformed with use of exponential line broadening in ω_2 and Kaiser window functions in ω_1. The first point in each dimension was halved before Fourier transformation;[79] additional baseline corrections were unnecessary. Zero filling was employed prior to transformation such that the final spectra contained 4K × 4K real data points.

Relaxation rate constants and NOE enhancements were calculated from peak heights of the heteronuclear resonances. Data analysis was performed on a Convex C2 computer with programs written in Fortran 77; commercial[80] and published[81] numerical algorithms were used as applicable. The longitudinal relaxation rates were obtained by a three-parameter nonlinear optimization of eq 1; the transverse relaxation rate was obtained by a two-parameter nonlinear optimization of eq 2. The NOE enhancements were calculated from eq 3; the average values of η and standard errors in the mean were determined from four independent experiments.

Curve fitting used the Levenburg–Marquardt algorithm[81] to minimize the value of χ^2, given by

$$\chi^2 = \sum_{i=1}^{n} [I(T_i) - \hat{I}(T_i)]^2/\sigma^2 \qquad (16)$$

In eq 16, $I(T_i)$ is the experimental peak intensity; $\hat{I}(T_i)$ is the intensity predicted from the values of the adjustable parameters in the model function, at the ith time point; σ is the uncertainty in the experimental data points; and n is the number of time points recorded.

The uncertainties in the measured peak heights, σ_h, were set equal to the root-mean-square baseline noise in the spectra. This assumption was validated by recording two duplicate spectra with use of the sequence of Figure 1b with T = 0.02 s. Assuming that the peak heights of the 24 C^α resonances are identically distributed, the standard deviation of the differences between the heights of corresponding peaks in the paired spectra is equal to $2^{1/2}\sigma_h$. The value of σ_h determined in this manner was compared to the root-mean-square baseline noise.

Statistical analyses of the results of the non-linear optimizations of eqs. 1 and 2 were performed using Monte Carlo simulations of the distributions of the peak intensities and optimized parameters.[81–83] The predicted peak intensities, calculated with eq 1 or 2 and the values of the optimized parameters, were assumed to be the means of Gaussian distributions with standard deviations equal to σ_h. Five hundred simulated data sets were chosen at random from these distributions and fit with eq 1 or 2. The statistical properties of the resultant simulated distributions of the peak intensities and relaxation parameters were assumed to be equal to the properties of the actual distributions.

Uncertainties in the optimized parameters were obtained from the covariance matrix of the optimized model and validated by comparison to the Monte Carlo simulation results. The sufficiency of the monoexponential decay functions given by eqs 1 and 2 and the accuracy of the value of σ used in eq 16 were evaluated with a χ^2 goodness-of-fit test.[81,82] The test statistic was the residual χ^2 value from the Levenburg–Marquardt optimization of eq 1 or 2. Although this statistic is only approximately distributed as a χ^2 variable because the model functions are nonlinear, the Monte Carlo simulations indicated that the critical values of the distribution of the test statistic were similar to the critical values for an exact χ^2 variable with p parameters and $\nu = n - p$ degrees of freedom. For the R_1 measurements, ν = 6 and the α = 0.05 critical value for the exact χ^2 statistic is 12.59; for the R_2 measurements, ν = 8 and the critical value is 15.51.[84] A value of the residual χ^2 for a single relaxation curve that is greater than the critical value indicates with 95% confidence that the model function or the value of σ does not adequately describe the data.

Global measures of the sufficiency of eqs 1 and 2 and σ in describing the relaxation data for Xfin-31 also were obtained from the sum of the residual χ^2 values obtained from fitting the R_1 or R_2 data for all the methine carbons in Xfin-31, under the assumption that the residual χ^2 for individual resonances are drawn from the same distribution. The sum of the m individual residual χ^2 values is distributed as a χ^2 variable with $\nu = m(n - p)$ degrees of freedom and was tested as described above by using the critical values for exact χ^2 distributions. For the R_1 measurements, ν = 162 and the α = 0.05 critical value is 192.7; for the R_2 measurements, ν = 216 and the critical value is 236.7.[84]

In theory, calculation of the model free parameters from the measured relaxation parameters with eqs 4, 5, and 8–13 necessitates finding the roots of a system of nonlinear functions in the presence of observational noise. As this problem is mathematically intractable, model free parameters were obtained from the relaxation rate constants and NOE enhancements by minimization of the target function

$$\chi^2 = \sum_{i=1}^{r} \Gamma_i^2 = \sum_{i=1}^{r} [(R_{1i} - \hat{R}_{1i})^2/\sigma_{1i}^2 + (R_{2i} - \hat{R}_{2i})^2/\sigma_{2i}^2 + (\eta_i - \hat{\eta}_i)^2/\sigma_{\eta i}^2] \qquad (17)$$

in which Γ_i^2 is the sum of the squared residuals; R_{1i}, R_{2i}, and η_i are the experimental values of the relaxation parameters; σ_{1i}, σ_{2i}, and $\sigma_{\eta i}$ are the uncertainties in the relaxation parameters; and $\hat{R}_{1i}$, $\hat{R}_{2i}$, and $\hat{\eta}_i$ are the values calculated with eqs. 4, 5, 8–15, for the ith methine ^{13}C nucleus. The summation extends over the r nuclei included in the calculation. Despite the formal similarity of this approach to curve fitting by χ^2 minimization, values of the parameters that minimize the target function are not necessarily equivalent estimators of the roots of the nonlinear equations.[82]

In the first instance, model free parameters were calculated assuming that the dipolar interaction was the predominant relaxation mechanism; thus, R_a in eq 5 and $\Delta\delta$ in eqs 11–13 were set equal to zero. In the second analysis, both dipolar and CSA relaxation mechanisms were included in

(75) Marion, D.; Wüthrich, K. *Biochem. Biophys. Res. Commun.* **1983**, *113*, 967–974.
(76) Live, D. H.; Davis, D. G.; Agosta, W. C.; Cowburn, D. *J. Am. Chem. Soc.* **1984**, *106*, 1939–1941.
(77) Bax, A.; Subramanian, S. *J. Magn. Reson.* **1986**, *67*, 565–569.
(78) Bigler, P. *J. Magn. Reson.* **1987**, *75*, 162–166.
(79) Otting, G.; Widmer, H.; Wagner, G.; Wüthrich, K. *J. Magn. Reson.* **1986**, *66*, 187–193.
(80) IMSL, Houston TX.
(81) Press, W. H.; Flannery, B. P.; Teukolsky, S. A.; Vetterling, W. T. *Numerical Recipes*; Cambridge University Press: Cambridge, 1986.
(82) Ratkowsky, D. *Nonlinear Regression Modeling*; Marcel Dekker: New York, 1983; pp 143–151.
(83) Borowiak, D. S. *Model Discrimination for Nonlinear Regression Models*; Marcel Dekker: New York, 1989; pp 55–167.
(84) Devore, J. L. *Probability and Statistics for Engineering and the Sciences*; Brooks/Cole: Monterey CA, 1982.

eqs 11–13 and R_a was set equal to zero in eq 5. A third analysis was performed to examine the effects of other contributions to the apparent spin–spin relaxation rate constants on the values of the model free parameters. This calculation was similar to the first except that R_a was included in eq 5 as a free parameter for those carbon nuclei that had R_2/R_1 ratios that were more than one standard deviation greater than the average ratio. This criterion for including a contribution from R_a to R_2 for a given nucleus has been arbitrarily chosen; the present data are insufficient to establish statistically or experimentally which resonances are affected by decay processes other than dipolar relaxation or what additional mechanisms contribute to the apparent R_2 rate constants. Consequently, the results of the third analysis have been used only to indicate possible effects of nondipolar contributions to the apparent R_2 on the calculation of the model free parameters.

The optimization routine used quadratic interpolation[80,81] to globally optimize τ_m and a Levenburg–Marquardt algorithm that incorporated active-set strategy[85] to optimize S^2, τ_e, and R_a for each nucleus subject to the constraints $0 \le S^2 \le 1$, $0 \le \tau_e \le \tau_m$, and $0 \le R_a$. An initial estimate of τ_m was obtained from the average R_2/R_1 ratio for the backbone resonances and eq 15. Initial estimates of S^2 and τ_e were obtained for each methine carbon by a coarse grid search with τ_m held constant. The final values of the model free parameters were obtained for the backbone nuclei by iterative optimization of the initial estimates, including τ_m. The final values of S^2, τ_e, and R_a for the side chain nuclei were obtained by optimizing the initial estimates of these parameters with τ_m fixed at the global value determined for the backbone nuclei.

The uncertainties in the model free parameters were estimated by Monte Carlo simulations. The predicted values of the relaxation parameters, which were calculated from the optimized model free parameters, and the uncertainties in the measured relaxation parameters were assumed to be the means and standard deviations of Gaussian distributions; simulated sets of R_1, R_2, and η were obtained by random selection from these distributions. Five hundred simulated data sets were analyzed and the averages and standard deviations of the simulated model free parameters determined. The biases in the values of the model free parameters were defined as the differences between the optimized values of the parameters and the means of the simulated parameters. The uncertainties in the empirical values of the model free parameters are reported as the standard deviations of the simulated parameters.

The values of the constants used in eqs 8–15 are the following: $h = 6.626 \times 10^{-34}$ J s, $\mu_0 = 4\pi \times 10^{-7}$ T m A^{-1}, $\gamma_H = 2.6752 \times 10^8$ s^{-1} T^{-1}, $\gamma_C = 6.728 \times 10^7$ s^{-1} T^{-1}, $r_{CH} = 1.09 \times 10^{-10}$ m, $\omega_H = 2\pi \times 499.874$ MHz, $\omega_C = 2\pi \times 125.694$ MHz. A value of $\Delta\delta = 25$ ppm, which is typical of methine α-carbon nuclei,[86-89] was used for CSA calculations. With use of these constants, $D_{CH} = 1.46 \times 10^5$ s^{-1}, and the CSA constant $\Delta\delta\,\omega_C = 1.97 \times 10^4$ s^{-1}; consequently the contribution of CSA to the relaxation parameters is expected to be negligible.

Results

The assignments of the methine carbons in Xfin-31 are indicated in Figure 2, which is a contour plot of the (a) α and (b) side-chain resonances obtained by using the pulse sequence of Figure 1a and $T = 0.01$ s; complete resonance assignments for the protonated ^{13}C spectrum of Xfin-31 have been reported elsewhere.[90] The resonances of Lys^2 and His^{23} C$^\alpha$ are partially overlapped; however quantitative measurements of the intensity of each resonance were still possible. The resonances of Leu^5 C$^\gamma$ and Leu^{16} C$^\gamma$ are more severely overlapped; reliable intensity measurements could only be made for the narrower, more intense Leu^5 resonance. The Gly^4 methylene C$^\alpha$ resonance is suppressed by the DEPT polarization transfer and cannot be observed in these experiments. In total, relaxation parameters were measurable for 24 of the 25 backbone C$^\alpha$ resonances and 3 of the 4 side chain methine groups. The average DEPT efficiency was calculated to be 2.74 ± 0.28 for the methine resonances, as compared to a theoretical value of $\gamma_H/\gamma_C = 4$. The spectrum shown in Figure 2 was acquired in approximately 18 h.

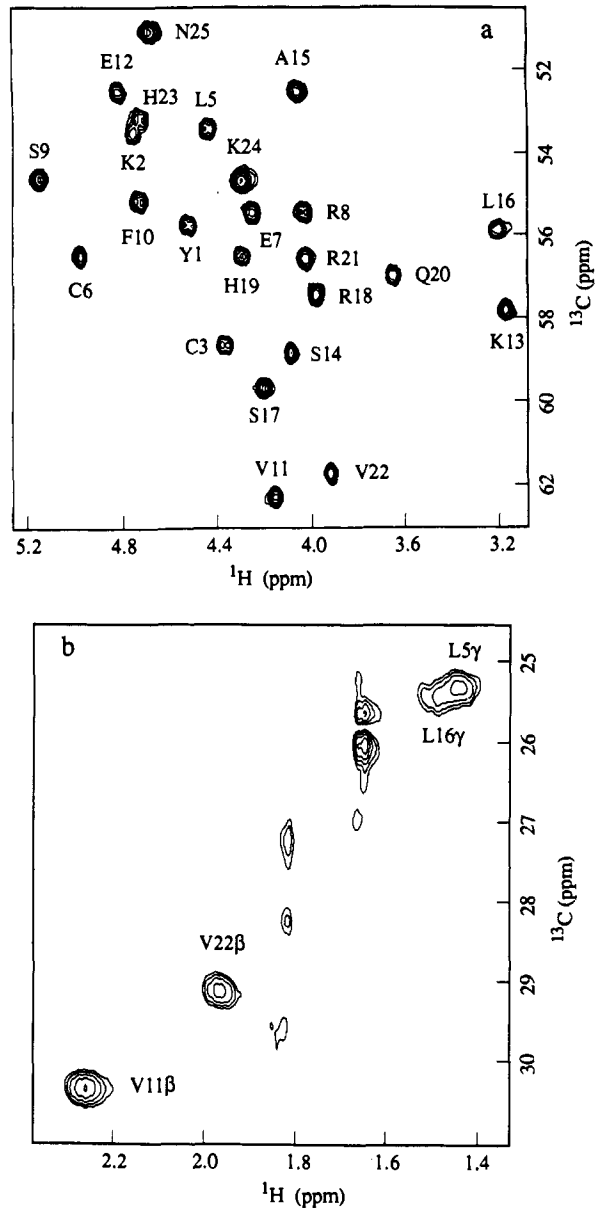

Figure 2. Double DEPT spectrum of Xfin-31 methine resonances. Shown are contour plots of regions of the heteronuclear correlation spectrum acquired with the pulse sequence of Figure 1a and $T = 0.10$ s that display the (a) backbone C$^\alpha$ and (b) side chain Val C$^\beta$ and Leu C$^\gamma$ resonances. The spectrum was acquired in approximately 18 h.

The phenomenological spin–lattice and spin–spin relaxation rate constants and the NOE enhancements calculated from the measured peak heights and root-mean-square baseline noise with eqs 1–3 and 16 are listed in Table I. The uncertainties in the values of R_1 and R_2 are the formal standard deviations calculated from the covariance matrix in the nonlinear optimization routine and are 5–10%; the uncertainties in η are calculated as the standard errors in the mean of four replicate measurements and are 10–25%. Monte Carloe simulations of the standard deviations of the optimized values of R_1 and R_2 agreed with the formal results to within 3%. Cross sections taken parallel to the ω_2 axis through the C$^\alpha$ resonance of Glu^{12} for the R_1 and R_2 relaxation experiments are shown in Figure 3 together with the optimized fits of the peak intensities to eqs 1 and 2. Signal-to-noise ratios were typically 30 for the initial data point in each experiment.

The appropriateness of the model functions given by eqs 1 and 2 and of the accuracy of the value of σ used in eq 16 were monitored by the χ^2 goodness-of-fit test. For example, inversion recovery curves of 27 methine resonances were analyzed by using eq 1; only one of these, His^{23} C$^\alpha$, gave an optimized fit with $\chi^2 = 12.1$ that was greater than its simulated critical value of 11.7.

(85) Gill, P. E.; Murray, W. *NPL Report NAC 72*; National Physics Laboratory: England, 1976.
(86) Naito, A.; Ganapathy, S.; Akasaka, K.; McDowell, C. A. *J. Chem. Phys.* **1981**, *74*, 3190–3197.
(87) Naito, A.; Ganapathy, S.; Raghunathan, P.; McDowell, C. A. *J. Chem. Phys.* **1983**, *79*, 4173–4182.
(88) Naito, A.; McDowell, C. A. *J. Chem. Phys.* **1983**, *81*, 4795–4803.
(89) Janes, N.; Ganapathy, S.; Oldfield, E. *J. Magn. Reson.* **1983**, *54*, 111–121.
(90) Lee, M. S.; Palmer, A. G.; Wright, P. E. Submitted for publication.

Table I. ^{13}C Relaxation Parameters for Xfin-31[a]

residue	R_1, s^{-1}	R_2, s^{-1}	η	R_2/R_1
		Backbone $^{13}C^{\alpha}$		
Tyr 1	3.72 ± 0.22	7.84 ± 0.41	0.34 ± 0.09	2.10 ± 0.17
Lys 2	4.23 ± 0.27	8.45 ± 0.52	0.18 ± 0.07	2.00 ± 0.18
Cys 3	4.27 ± 0.31	14.1 ± 1.2	0.32 ± 0.03	3.30 ± 0.36
Leu 5	4.15 ± 0.26	14.3 ± 1.0	0.28 ± 0.04	3.45 ± 0.32
Cys 6	4.12 ± 0.15	10.7 ± 0.4	0.23 ± 0.06	2.60 ± 0.13
Glu 7	3.92 ± 0.22	8.77 ± 0.54	0.26 ± 0.05	2.24 ± 0.19
Arg 8	4.35 ± 0.25	10.8 ± 0.6	0.28 ± 0.05	2.48 ± 0.21
Ser 9	4.32 ± 0.19	8.58 ± 0.35	0.29 ± 0.03	1.99 ± 0.12
Phe 10	3.80 ± 0.21	7.11 ± 0.37	0.25 ± 0.03	1.87 ± 0.14
Val 11	3.57 ± 0.15	8.77 ± 0.35	0.30 ± 0.06	2.46 ± 0.14
Glu 12	3.75 ± 0.20	7.96 ± 0.38	0.25 ± 0.06	2.12 ± 0.15
Lys 13	3.96 ± 0.20	7.87 ± 0.43	0.30 ± 0.02	1.99 ± 0.15
Ser 14	3.79 ± 0.12	11.2 ± 0.4	0.26 ± 0.03	2.97 ± 0.14
Ala 15	4.26 ± 0.23	8.63 ± 0.42	0.28 ± 0.05	2.02 ± 0.15
Leu 16	3.98 ± 0.28	8.94 ± 0.60	0.19 ± 0.04	2.25 ± 0.22
Ser 17	4.07 ± 0.16	9.31 ± 0.39	0.27 ± 0.03	2.28 ± 0.13
Arg 18	3.76 ± 0.18	9.80 ± 0.44	0.24 ± 0.03	2.61 ± 0.17
His 19	3.75 ± 0.23	9.74 ± 0.61	0.24 ± 0.03	2.60 ± 0.23
Gln 20	3.93 ± 0.28	12.2 ± 0.9	0.28 ± 0.02	3.11 ± 0.31
Arg 21	3.92 ± 0.19	8.31 ± 0.42	0.29 ± 0.02	2.12 ± 0.15
Val 22	3.81 ± 0.19	12.9 ± 0.7	0.33 ± 0.03	3.40 ± 0.24
His 23	3.48 ± 0.24	14.0 ± 1.0	0.27 ± 0.08	4.03 ± 0.41
Lys 24	3.58 ± 0.12	5.92 ± 0.17	0.64 ± 0.06	1.65 ± 0.07
Asn 25	2.50 ± 0.07	3.89 ± 0.10	0.79 ± 0.08	1.55 ± 0.06
		Side Chain Methine ^{13}C		
Val 11β	3.31 ± 0.20	6.46 ± 0.36	0.37 ± 0.08	1.95 ± 0.16
Val 22β	3.01 ± 0.23	10.7 ± 0.9	0.51 ± 0.06	3.55 ± 0.42
Leu 5γ	2.27 ± 0.18	5.56 ± 0.36	0.45 ± 0.07	2.45 ± 0.25

[a] No results are available for Gly[4], because the DEPT sequence used in the experimental protocols suppresses magnetization from the methylene C^{α}, or for the C^{γ} of Leu[16], because the resonance could not be resolved from that of Leu[5].

Table II. Model Independent Parameters for Xfin-31[a]

residue	S^2	τ_e	Γ_i^2
	Backbone $^{13}C^{\alpha}$		
Tyr 1	0.73 ± 0.04	61 ± 34	1.09
Lys 2	0.86 ± 0.03		4.65
Cys 3	0.89 ± 0.03		13.6
Leu 5	0.96 ± 0.06		18.1
Cys 6	0.97 ± 0.04		2.58
Glu 7	0.84 ± 0.04	36 ± 44	0.43
Arg 8	0.94 ± 0.08		0.69
Ser 9	0.84 ± 0.03		7.04
Phe 10	0.72 ± 0.03	17 ± 10	9.22
Val 11	0.80 ± 0.03	31 ± 24	0.62
Glu 12	0.77 ± 0.03	25 ± 22	2.34
Lys 13	0.78 ± 0.03	39 ± 11	4.76
Ser 14	0.92 ± 0.02		20.2
Ala 15	0.84 ± 0.03	67 ± 58	3.98
Leu 16	0.87 ± 0.04		0.90
Ser 17	0.88 ± 0.02	50 ± 50	0.33
Arg 18	0.88 ± 0.03	18 ± 23	1.90
His 19	0.87 ± 0.04	15 ± 25	0.87
Gln 20	0.95 ± 0.04		7.64
Arg 21	0.81 ± 0.03	41 ± 16	2.13
Val 22	0.91 ± 0.04		28.2
His 23	0.92 ± 0.05		22.8
Lys 24	0.48 ± 0.02	123 ± 16	16.3
Asn 25	0.28 ± 0.01	77 ± 7	17.4
	Side Chain Methine ^{13}C		
Val 11β	0.62 ± 0.03	37 ± 10	3.32
Val 22β	0.66 ± 0.04	78 ± 28	15.0
Leu 5γ	0.47 ± 0.03	27 ± 9	0.93

[a] Shown are the model free parameters S^2 and τ_e and the sum of the square residuals Γ_i^2 (eq 17) for the backbone and side chain methine ^{13}C spins of Xfin-31 that were calculated with $R_a = 0$ for all resonances. The overall rotational correlation time was determined to be 1.88 ± 0.02 ns. Results are not available for Gly[4], because the DEPT sequence used in the experimental protocols suppresses magnetization from the methylene C^{α}, or for the C^{γ} of Leu[16], because the resonance could not be resolved from that of Leu[5].

On average, one of every 20 residual χ^2 values should exceed the $\alpha = 0.05$ critical value. The sum of the residual χ^2 values for all resonances was 160.4 which is less than the critical value given above. Therefore the goodness-of-fit tests of the residual χ^2 values indicate that the root-mean-square baseline noise is an accurate representation of the uncertainties in the peak intensities and that the inversion recovery data are adequately described by eq 1.

On the other hand, CPMG decay curves for 9 of the 27 resonances had χ^2 values greater than the critical value when analyzed with eq 2, which indicates significant lack of fit between the model and the data for these resonances. Similarly, the sum of the residual χ^2 values for all resonances was 421.2, which is much greater than the critical value given above. Therefore the goodness-of-fit tests of the residual χ^2 values indicate that either the root-mean-square baseline noise is not an accurate representation of the uncertainties in the peak intensities or the CPMG data are not well described by eq 2. The simplest explanation is the former one; statistically discriminating between eq 2 and possible alternative model functions would require a significantly larger number of data points than are available. Assuming that eq 2 is satisfactory, the uncertainty in the peak intensities was estimated to be 1.4 times the root-mean-square baseline noise in the spectra by scaling the observed sum of the χ^2 values to equal the number of degrees of freedom, given above, and by using eq 16. The value of σ_h calculated from two duplicate spectra was within 5% of the root-mean-square baseline noise and had a 95% confidence interval that extended from 0.78 σ_h to 1.40 σ_h.[84] This confidence interval indicates that a large number of replicate spectra would be required to statistically ascertain whether the uncertainties in the peak heights were better estimated by 1.0 or 1.4 times the root-mean-square baseline noise. Nonetheless this analysis suggests that, subject to the above assumptions, the uncertainties in the values of R_2 given in Table I may be underestimated by up to a factor of 1.4.

As discussed above, processes such as translational diffusion and chemical exchange can systematically contribute to R_2. For macromolecules, the diffusional contribution to R_2 (eq 5) can be minimized with millisecond spin–echo periods. With use of eq 7, the diffusional contribution to the apparent relaxation for the methine carbons in Xfin-31 is estimated to be <1% from the dependence of the relaxation rate constant of ^{13}C-labeled alanine on the spin–echo period and the relative translational diffusion coefficients of alanine and Xfin-31 (data not shown). As shown by eq 6, the CPMG sequence also minimizes the effect of chemical exchange on the apparent relaxation if $\xi k_{ex} \ll 1$; in the present case, $\xi = 2.5$ ms, and k_{ex} must be greater than approximately 40 s^{-1} for chemical exchange to contribute significantly to the apparent spin–spin relaxation rate.

For comparison, relaxation parameters were also determined from the integrated volumes of the resonances in spectra processed with Lorentzian-to-Gaussian transformation in ω_2. Values of the relaxation parameters determined with use of peak volumes agree with the values determined with use of peak heights; however the relative precisions of the parameters are approximately 10–50% lower (data not shown).

The values of R_2/R_1 for the methine resonances are listed in Table I; the average value for the 24 backbone resonances is 2.46 ± 0.62 and the initial estimate of τ_m calculated with eq 15 is 1.92 ± 0.09. The values of R_2/R_1 for Lys[24] and Asn[25] are more than one standard deviation smaller than the average, which indicates that the S^2 is small enough and τ_e large enough to appreciably affect the bracketed term in eq 15. The C^{α} resonances of Cys[3], Leu[5], Ser[14], Gln[20], Val[22], and His[23] and the C^{β} of Val[22] have $R_2/R_1 \geq 3$, which may indicate that decay processes other than dipolar relaxation are contributing to the apparent R_2 for these nuclei (eq 5).

The resultant values of the model free parameters S^2 and τ_e calculated assuming purely dipolar relaxation are listed in Table II; values of S^2, τ_e, and R_a determined assuming dipolar relaxation augmented by R_a for nuclei with $R_2/R_1 \geq 3$ are given in Table III. The global value of τ_m determined for the backbone resonances is 1.88 ± 0.02 ns for the former analysis and 1.74 ± 0.03

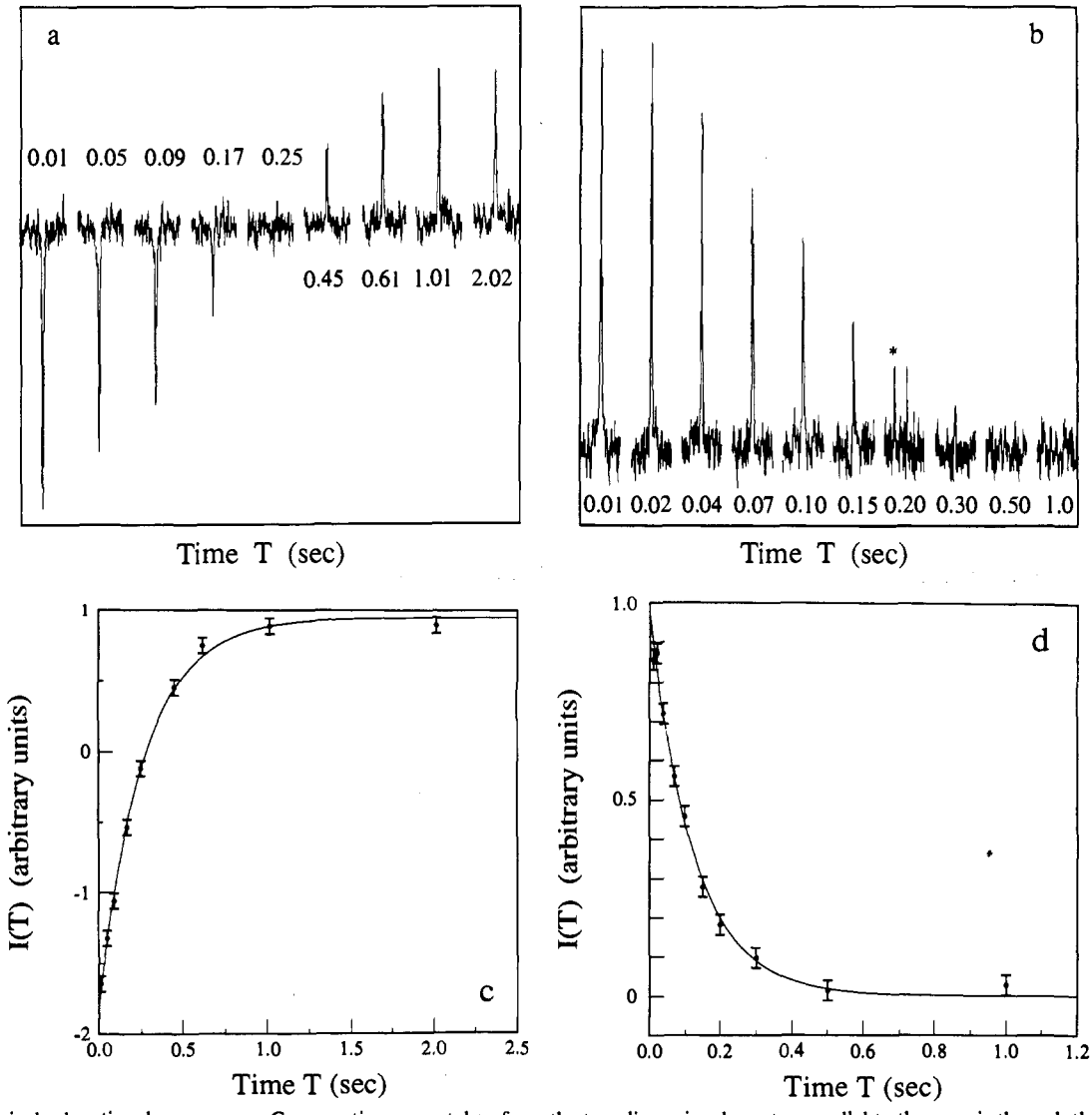

Figure 3. Typical relaxation decay curves. Cross sections were taken from the two-dimensional spectra parallel to the ω_2 axis through the C^α resonance of Glu^{12}. Shown in (a) are the cross sections for the inversion recovery measurements with use of the sequence of Figure 1a. Shown in (b) are the cross sections for the CPMG measurements with use of the sequence of Figure 1b. The feature marked * in (b) is a spurious noise peak. The parametric relaxation delay T is shown for each cross section. The optimized nonlinear fits of eqs 1 and 2 to the data in (a) and (b) are shown in (c) and (d), respectively. The uncertainty in the peak heights is equal to the root-mean-square baseline noise in the spectra.

ns for the latter. As expected from the relative magnitude of the dipolar and CSA contributions to the relaxation rate constants, the values of the model free parameters were not significantly affected by inclusion of CSA contributions to the relaxation parameters and are not tabulated. The concordance between the experimental values of the relaxation parameters and the values calculated from the optimized model free parameters was not formally tested statistically; additional investigations of the statistical properties of the estimators of the model free parameters obtained by minimization of eq 18 are in progress. Empirically, all three of the calculated relaxation parameters for a given carbon nucleus agreed with the measured parameters within an approximate 95% confidence interval, given by 1.96 times the measured uncertainties in the parameters (Table I), if $\Gamma_i^2 < 5$ (Tables II and III). The largest discrepancies between the experimental and calculated parameters were observed for resonances with $R_2/R_1 \geq 3$ when R_a was not included in eq 5 and for the two C-terminal residues. The large values of Γ_i^2 obtained for the C-terminal residues, Lys^{24} and Asn^{25}, are consistent with the observation that these two nuclei have the largest χ^2 values from the fit of eq 2 to the CPMG decay data.

The values of S^2 for those nuclei with $R_2/R_1 \geq 3$ were smaller by 0.10 ± 0.06 unit when R_a was included in the analysis, but the order parameters for the other nuclei were not significantly affected. Thus, the order parameters for nuclei whose apparent R_2 contains contributions from conformational exchange, or other first-order rate processes, may be slightly overestimated by the simplest model free formalism.

As indicated in Tables II and III, the Monte Carlo simulations estimated the precision in the values of S^2 as approximately 5% and the precision in the values of R_a as 20–40%. The precision in the values of τ_e depended strongly on the values of S^2: if $S^2 < 0.7$, the uncertainties in τ_e were 10–30%; if $0.7 \leq S^2 \leq 0.8$, the uncertainties in τ_e were 25–100%; and if $S^2 < 0.8$ the uncertainties in τ_e were on the order of 100% for only a few resonances. Most of the nuclei with $S^2 > 0.8$ had mean values of τ_e from the simulations that were strongly biased compared to the optimized values or had residual values of $\Gamma_i^2 > 5.0$, which suggests that the numerical optimization of τ_e may be unreliable in these cases. Accordingly, a value for τ_e has been reported for a nucleus with $S^2 > 0.8$ only if approximate 95% confidence intervals for the three relaxation parameters calculated from the model free parameters encompassed the experimental values and the simulations indicated that the calculation of τ_e was unbiased. The average value of $\tau_e = 34 \pm 16$ ps for the ten interior residues for which values of τ_e are reported in Table II, and the average value of $\tau_e = 29 \pm 17$ ps for the 10 interior residues for which τ_e have been reported in Table III.

Graphs of the values of S^2 taken from Tables II and III for the C^α of each residue in Xfin-31 are shown in Figure 4. As

Table III. Model Independent Parameters and R_a for Xfin-31[a]

residue	S^2	τ_e	R_a	Γ_i^2
		Backbone $^{13}C^{\alpha}$		
Tyr 1	0.75 ± 0.04	52 ± 34		0.03
Lys 2	0.87 ± 0.04			1.80
Cys 3	0.88 ± 0.03		4.9 ± 1.2	0.00
Leu 5	0.88 ± 0.05		5.3 ± 1.0	0.00
Cys 6	0.97 ± 0.05			10.4
Glu 7	0.85 ± 0.04	26 ± 32		0.06
Arg 8	0.98 ± 0.09			2.47
Ser 9	0.86 ± 0.03	64 ± 35		2.02
Phe 10	0.74 ± 0.03	14 ± 12		4.25
Val 11	0.81 ± 0.03	16 ± 22		4.29
Glu 12	0.79 ± 0.03	15 ± 18		0.24
Lys 13	0.80 ± 0.03	37 ± 10		1.32
Ser 14	0.82 ± 0.02	17 ± 14	2.9 ± 0.6	0.00
Ala 15	0.86 ± 0.04			0.94
Leu 16	0.88 ± 0.04			0.85
Ser 17	0.89 ± 0.03			0.54
Arg 18	0.88 ± 0.03			6.56
His 19	0.88 ± 0.04			3.28
Gln 20	0.84 ± 0.06		3.6 ± 1.2	0.00
Arg 21	0.82 ± 0.03	37 ± 18		0.13
Val 22	0.78 ± 0.04	51 ± 45	4.8 ± 0.8	0.00
His 23	0.74 ± 0.06	17 ± 22	6.4 ± 1.1	0.00
Lys 24	0.50 ± 0.02	118 ± 15		8.02
Asn 25	0.30 ± 0.02	73 ± 8		9.60
		Side Chain Methine ^{13}C		
Val 11β	0.63 ± 0.03	36 ± 11		0.93
Val 22β	0.55 ± 0.05	54 ± 16	4.6 ± 1.0	0.00
Leu 5γ	0.48 ± 0.03	26 ± 9		2.81

[a] Shown are the model free parameters S^2 and τ_e, R_a, and the sum of the square residuals Γ_i^2 (eq 17) for the backbone and side chain methine ^{13}C spins of Xfin-31. R_a was included as a free parameter only for those nuclei for which $R_2/R_1 \geq 3$; R_a was taken to be zero for all other nuclei. The overall rotational correlation time was determined to be 1.74 ± 0.03 ns. Results are not available for Gly[4], because the DEPT sequence used in the experimental protocols suppresses magnetization from the methylene C^{α}, or for the C^{γ} of Leu[16], because the resonance could not be resolved from that of Leu[5].

indicated by the values of S^2 from Table II, four consecutive residues in the interior of the chain appear to have slightly lower order parameters than average. The average value of S^2 for the interior residues 2–9 and 14–23 is 0.89 ± 0.05 and the average value of S^2 for residues 10–13 is 0.77 ± 0.03. Thus, the average S^2 for residues 10–13 is significantly lower than that for the other interior residues with use of a two-sample t test with a level α = 0.05.[84] Similar treatment of the results of Table III gives an average value of S^2 = 0.87 ± 0.06 for the interior residues 2–9 and 15–23 and an average value of S^2 = 0.79 ± 0.03 for residues 10–14. Again, the average S^2 for residues 10–14 is significantly lower than that for the other interior residues.

As discussed above, the uncertainties in the values of R_2 may be underestimated by up to 40%; therefore, as a control, the model-free parameters also were determined by using the larger estimates of the uncertainties in R_2. The root-mean-square deviation between the two values of S^2 for each resonance is 0.02, and the uncertainties in the values of S^2 increase by approximately 12%; however, none of the qualitative trends observed in the order parameters are affected. Consequently, the analysis appears to be relatively insensitive to the differences in estimated uncertainties for the peak intensities from the CPMG experiments.

Discussion

The ^{13}C spin–lattice and spin–spin relaxation rates and the heteronuclear $\{^1H\}$–^{13}C NOE enhancements have been measured for 27 of the 28 methine carbons in the Xfin-31 zinc finger and analyzed with a model free formalism to characterize the amplitudes and time scales of the internal motions. As the experiments described herein are relatively new and the statistical properties of the analytical methods used to interpret them are difficult to establish, extensive use has been made of Monte Carlo simulations to assess the magnitudes of the uncertainties in the resonance intensities, relaxation rate constants, and model free

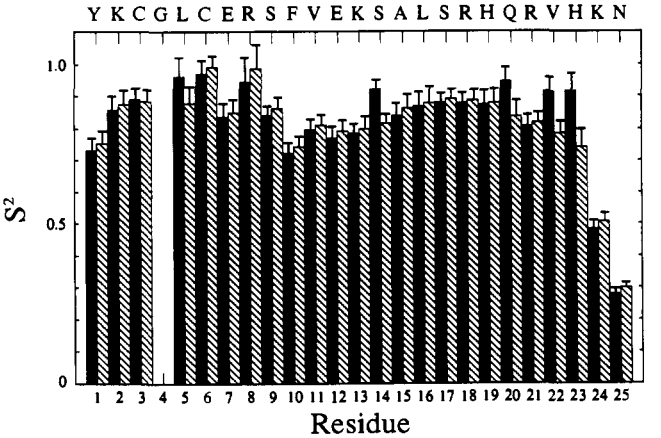

Figure 4. Order parameters for the C^{α} methine groups in Xfin-31. The values of S^2 given in Table II (solid) and Table III (hatched) are plotted versus the amino acid sequence of Xfin-31. The error bars indicate the uncertainties estimated from Monte Carlo simulations. No data are available for Gly[4] because the C^{α} resonance is suppressed by the DEPT sequence.

parameters and to detect systematic deviations from the models assumed in eqs 1, 2, and 14.

Not unexpectedly, the CPMG relaxation results are more subject to discordance between the experimental data and the model function than are the inversion recovery measurements; the statistical analysis emphasizes that detecting systematic deviations between experimental data and exponential model functions requires a large number of data points distributed over the entire recovery curve. The heteronuclear NOE enhancements are the measured quantities with the highest relative standard deviations; duplicate measurements of the enhancements are therefore vital to minimizing uncertainties in subsequent analyses of the relaxation parameters.

The object of heteronuclear relaxation studies of proteins is to obtain information on the spectral density functions of the C–H bond vectors and hence insight into the characteristics of the internal motions of the molecule. The relaxation data for most resonances could be fit by the simple model free formalism based on the spectral density function given by eq 14. In the present study, internal motions for which $\tau_e < 75$ ps are in the fast motion regime as defined by Lipari and Szabo[36] and should be well represented by the simplest formalism. As shown in Table II, this condition is satisfied for all nuclei for which τ_e could be determined, except for Lys[24]. Monte Carlo simulations indicated that determination of τ_m and S^2 from the relaxation parameters is numerically robust, but determination of τ_e frequently is unreliable for resonances with $S^2 > 0.8$.

For the seven methine carbons with R_2/R_1 ratios that were much larger than average (Table I), values of the model free parameters could not be found that would fit the systematically large R_2 simultaneously with the unbiased values of R_1 and η (Table II); inclusion of an additional R_a term (Table III) suggests that these resonances may be affected by decay processes other than dipolar relaxation. Six of these nuclei occur in residues that either are zinc ligands or are adjacent to zinc ligands. This strongly suggests the presence of some, as yet unidentified, conformational exchange process involving the zinc binding site. The NMR resonance of the amide proton of Leu[5] is also very broad even though the amide proton exchanges slowly with solvent.[91] The exchange process must be rapid compared to the chemical shift difference between the conformers because only one resonance is observed for each spin; however the intrinsic exchange rate constant cannot be estimated because, even for the simple process

(91) Lee, M. S. Unpublished results.
(92) Shaka, A. J.; Barker, P. B.; Freeman, R. *J. Magn. Reson.* **1985**, *64*, 547–552.
(93) Shaka, A. J.; Keeler, J.; Frenkiel, T.; Freeman, R. *J. Magn. Reson.* **1983**, *52*, 334–338.

described by eq 6, the calculated exchange rate depends strongly on the frequency difference between the two conformers, which is not presently known. Further experiments are in progress to confirm the existence of the exchange process and investigate its molecular basis.

The principal components of the inertial tensor of Xfin-31 are calculated from the NMR structure[65] to be in the ratio 1.00:1.43:1.84 and therefore the molecule might not be expected to undergo isotropic rotational motion. Nonetheless, the relaxation results were adequately described by a single rotational correlation time, which suggests that the analysis is insensitive to moderately anisotropic rotational motions.

As shown by the order parameters listed in Table II and shown graphically in Figure 4, motions of the backbone of Xfin-31 are highly restricted except for the C- and N-termini. The N-terminal residue Tyr^1 has an S^2 that is smaller by only 0.15 unit relative to the order parameters for the interior backbone residues, which indicates that the β-sheet identified in the three-dimensional structure of Xfin-31 extends to the terminal residue. The C-terminal displays a sudden drop in S^2 from nearly 0.9 to 0.5 at residue Lys^{24}, which indicates that the helix observed between residues 12–24 in the three-dimensional structure of Xfin-31 is flexible at the last residue. No systematic differences in the values of the order parameters for residues in the helix and the β sheet could be discerned. As discussed above, the values of the order parameters for residues 10–13 are slightly, but with statistical significance, lower than those for the remainder of the interior backbone residues. In the three-dimensional structure of the molecule, these residues form a small loop between β-sheet and helical secondary structures. The results thus indicate that the loop is slightly more flexible than the secondary structural elements adjacent to it. Similar conclusions are obtained from the results given in Table III, except that the more flexible interior region of the backbone comprises residues 10–14 and the decrease in order parameters near the C-terminus is evident for Val^{22} and His^{23} as well as for Lys^{24} and Asn^{25}.

Measurements of ^{13}C heteronuclear relaxation offer a potential advantage, compared to ^{15}N measurements, in that side chain dynamics can be probed. For proteins at natural ^{13}C abundance, currently available pulse sequences can only be applied to the relaxation side chain methine and aromatic ring carbon nuclei.[55] For Xfin-31, relaxation parameters were determined for three of the four side chain methine groups. Although the results are too limited to draw general conclusions, the data are consistent with previous studies that have concluded that the values of S^2 decrease in the order $C^\alpha > C^\beta > C^\gamma$.[38,54] If the side chain motions are independent of the backbone motions and if free rotation occurs about the χ torsion angles, the S^2 for a side chain methine group should be reduced by a factor of 0.111 compared to the C^α nucleus for each intervening χ torsion angle.[38] As can be seen, the values of S^2 for the side chain are only reduced by a factor of approximately 0.7 for each χ torsion angle. These results indicate that the motions of the hydrophobic side chains, even in a polypeptide as small as Xfin-31, are substantially restricted.

As shown in Table II, reliable values of τ_e were obtained for the terminal, side chain, and 10 of the internal backbone resonances. The C^α of the N- and C-terminal residues appear to have values of τ_e that are longer than the values for the interior backbone resonances; however τ_e is influenced by both the amplitudes and rates of the microscopic internal motional processes, and consequently, detailed interpretation of the internal correlation times is not feasible. The use of molecular dynamics simulations for the interpretation of τ_e is currently under investigation.

Conclusion

The development of proton-detected heteronuclear correlation NMR experiments has led to a resurgence of interest in investigations of the relaxation of heteronuclei to characterize the rates and amplitues of the internal motions in proteins. In the present work, spin–lattice and spin–spin relaxation rate constants and NOE enhancements have been measured for the methine resonances in the zinc finger Xfin-31. The relaxation parameters have been interpretated by using a model free theory[36] to determine the overall rotational correlation time of the molecule and the order parameter and internal effective correlation time for the motions of each carbon nucleus. The patterns of internal motions that are observed for the backbone methine groups of Xfin-31 are similar to the patterns observed for the internal motions of the backbone amide groups of staphylococcal nuclease[61] and interleukin-1β[62] measured by ^{15}N heteronuclear NMR spectroscopy. The results obtained for the side chain methine groups in Xfin-31 provide initial results on motions inaccessible to study by ^{15}N NMR; the development of experimental protocols for proton-detected relaxation measurements of methylene and methyl ^{13}C spins will provide additional insight into the internal motions of proteins.

Acknowledgment. This work was supported by grants from the National Institutes of Health (GM 40089 and GM 36643). A.G.P. was supported by a National Science Foundation Postdoctoral Fellowship in Chemistry awarded in 1989 (CHE-8907510). We thank Min Lee for providing us with peptide samples and John Cavanagh, Pearl Tsang, and Jon Waltho for helpful discussions.